Pure & Appl. Chem., Vol. 69, No. 6, pp. 1179–1186, 1997.
Printed in Great Britain.

Excitons in semiconductor nanostructures with disorder

R. Zimmermann, F. Große and E. Runge

Max-Planck-AG "Halbleitertheorie" an der Humboldt-Universität zu Berlin
Hausvogteiplatz 5-7, D-10117 Berlin, FRG

Abstract: Excitons in quantum structures with alloy as well as interface disorder are treated. The optical properties follow from a solution of the Schrödinger equation describing the exciton center-of-mass motion. The absorption linewidth is always smaller than the underlying potential variation (motional narrowing). Using a kinetic approach with acoustic phonon scattering, luminescence lineshapes are calculated showing non-equilibrium exciton distributions. Spatially resolved spectroscopy allows to extract information on individual exciton eigenstates.

INTRODUCTION

Excitons have been found to determine the optical properties of a wide variety of solid state systems. In semiconductor physics, quantum structures are of particular importance since their design allows to concentrate on specific properties which are not available within bulk samples. The confinement of electrons and holes due to the energetic band edge variation between well and barrier material leads to a dramatic strengthening of the excitonic features [1]. Thus, undoped semiconductor quantum structures are an ideal playground for exciton physics. However, the definition of the interfaces on an atomic scale is never as ideal as theory would like to have it. Even with the highly sophisticated molecular beam epitaxy (MBE), interface fluctuations of a few monolayers (ML) can be hardly avoided. A further source of disorder is alloy fluctuation since most quantum structures have a ternary compound in the barrrier or in the well. These disorder effects determine the inhomogeneous part of the exciton line seen in optical measurements and even tend to dominate their linewidth in narrow quantum structures. Rather than considering this as an unwanted feature, the exciton linewidth in photoluminescence (PL) is usually taken as a quality measure of the growth process. A further indicator is the Stokes shift between the peaks in PL and absorption (or rather photoluminescence excitation, PLE).

The theoretical investigations and simulation results of the present paper aim at a quantitative under-

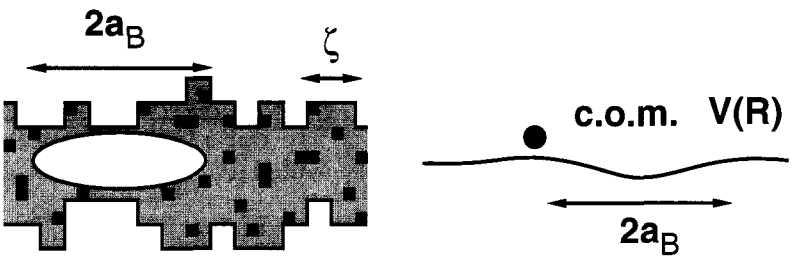

Fig. 1: Schematic view of the exciton in a ternary QW with rough interfaces (left) and the resulting correlated COM potential (right).

standing of the relation between growth-induced disorder effects and optical spectra in semiconductor quantum wells (QW). We have developed elsewhere a Monte Carlo simulation of the MBE growth of QWs which provides the necessary input for the subsequent exciton calculation [2]. Here we show that alloy disorder and roughness of the barrier-well interface contribute differently to the random potential of the exciton center-of-mass (COM) motion. Due to the averaging by the exciton relative motion the potential is correlated at least over distances of the exciton Bohr radius a_B, but reduced in energetic variation (Fig. 1). Solving the Schrödinger equation in this disordered potential landscape [3] gives directly the optical density (OD) of the $1s$ exciton as seen e.g. in absorption. More important for a comparison with experiment are luminescence spectra. Due to disorder, at low temperatures the excitons do not reach thermal equilibrium within their lifetime, and the PL lineshape deviates strongly from the OD. Therefore, a kinetic equation for scattering with acoustic phonons is derived using the disordered eigenstates as basis. A "relaxation mobility edge" shows up clearly in the distribution over energy, dividing the region of dominating band transport from that of hopping character. The calculated Stokes shift shows a non-monotonic temperature dependence in agreement with recent experiments. The kinetic approach can be easily modified to describe PLE which is shown to deviate markedly from the OD below the relaxation mobility edge, putting doubts on the usual assignment of PLE with OD. Finally, experimental micro-photoluminescence spectra are discussed as providing a fingerprint of individual disorder eigenstates.

CENTER OF MASS EXCITON EQUATION

The exciton Schrödinger equation in effective mass approximation

$$\left(-\frac{\hbar^2}{2m_e}\Delta_{\mathbf{r}_e}-\frac{\hbar^2}{2m_h}\Delta_{\mathbf{r}_h}-\frac{e^2/\epsilon_0}{|\mathbf{r}_e-\mathbf{r}_h|}+W_e(\mathbf{r}_e)+W_h(\mathbf{r}_h)-\mathcal{E}_\alpha\right)\Psi_\alpha(\mathbf{r}_e,\mathbf{r}_h)=0 \tag{1}$$

is supplemented by confinement potentials $W_a(\mathbf{r}_a)$ $(a=e,h)$ which describe the spatial variation of the local band edges. Having in mind a GaAs QW inbetween $Al_xGa_{1-x}As$ barriers, it is only the position of the Al atoms which defines the structure. Both alloy disorder and imperfect interface are coded into the Al occupation $\eta(\mathbf{r})=1$ resp. 0, and we put $W_a(\mathbf{r})=E_a^{\mathrm{GaAs}}+\Delta_a\,\eta(\mathbf{r})$ with the band edge difference Δ_a of the binary materials.
If the exciton binding energy is well below the disorder-induced broadening we can concentrate on the lowest bound state $1s$ and factorize the total wave function into

$$\Psi_\alpha(\mathbf{r}_e,\mathbf{r}_h)=u_e(z_e)\,u_h(z_h)\,\phi_{1s}(\boldsymbol{\rho}_e-\boldsymbol{\rho}_h)\,\psi_\alpha(\mathbf{R}) \tag{2}$$

introducing the 2D center-of-mass coordinate $\mathbf{R}=(m_e\boldsymbol{\rho}_e+m_h\boldsymbol{\rho}_h)/M$ with the exciton kinetic mass $M=m_e+m_h$. Both the confinement wave functions $u_a(z_a)$ and the relative wave function $\phi_{1s}(\boldsymbol{\rho})$ obey Schrödinger equations of the in-plane averaged QW structure with local Al concentration $x(z)=\langle\eta(\mathbf{R},z)\rangle$. Finally one is left with the COM equation

$$\left(-\frac{\hbar^2}{2M}\Delta_{\mathbf{R}}+V(\mathbf{R})\right)\psi_\alpha(\mathbf{R})=\mathcal{E}_\alpha\,\psi_\alpha(\mathbf{R})\,. \tag{3}$$

The random COM potential

$$V(\mathbf{R})=\int d\mathbf{R}'\sum_{a=e,h}\beta_a^2\,\phi_{1s}^2(\beta_a(\mathbf{R}-\mathbf{R}'))\int dz\,u_a^2(z)\,\Delta_a\,[\eta(\mathbf{R}',z)-x(z)] \tag{4}$$

is spatially correlated over the exciton Bohr radius a_B but scaled differently for electron and hole ($\beta_e=M/m_h$, $\beta_h=M/m_e$). Equations (3) and (4) are the starting point for calculations on simulated structures. Note that the $1s$ exciton energy $\hbar\omega_x$ of the averaged QW is taken as zero of energy in what follows. For dipole-allowed transitions, the exciton oscillator strength is related to the probability to find electron and hole at the same position,

$$\int d\mathbf{r}\,\Psi_\alpha(\mathbf{r},\mathbf{r})=\int dz\,u_e(z)\,u_h(z)\cdot\phi_{1s}(0)\cdot\int d\mathbf{R}\,\psi_\alpha(\mathbf{R})\,, \tag{5}$$

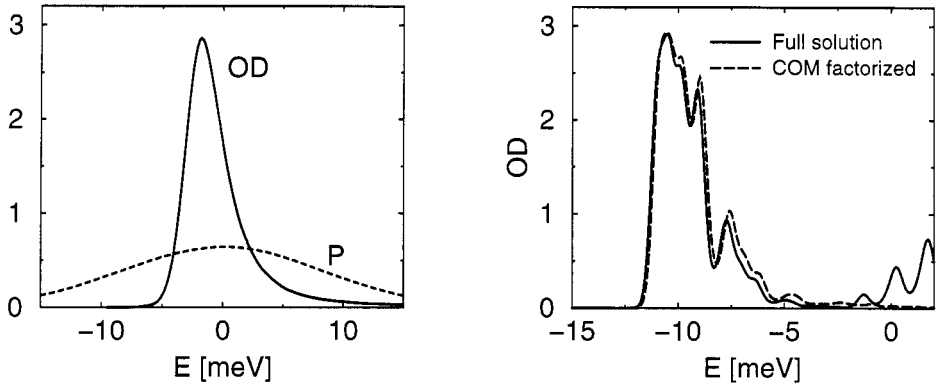

Fig. 2: Calculated optical density (OD) of a 10 ML $Al_{.3}Ga_{.7}As$ quantum well (L_z = 2.8 nm). Left: Motional narrowing of the OD compared to the COM potential distribution P (σ =8 meV). Right: Optical density of a 160 x 160 nm area generated via MBE growth simulation. Solid curve – full solution of the in-plane exciton equation, dashed curve – factorization of the COM motion.

and dropping constant prefactors the optical density is given by

$$D(\omega) = \sum_{\alpha} M_{\alpha}^2 \, \pi \, \delta(\hbar\omega - \mathcal{E}_{\alpha}) \; ; \quad M_{\alpha} = \int d\mathbf{R} \, \psi_{\alpha}(\mathbf{R}) \; . \tag{6}$$

We have shown elsewhere [3] that the calculated OD is slightly asymmetric towards higher frequencies and exhibits a reduced width compared to the underlying Gauss potential distribution. This has been called motional narrowing due to the COM motion, as found before in the study of 1D excitons [4]. Whereas these results had been obtained on artificially generated potentials (Fig. 2, left), we have implemented recently a simulation of the MBE crystal growth in order to get more realistic structures [2]. In the right part of Fig. 2 the calculated optical density is displayed, based on a simulation of a 10 monolayer QW (growth rate 1 ML/s, growth temperature 870 K). The disorder is found in the generated Al occupation $\eta(\mathbf{r})$. Deep in the barriers, the Al atoms tend to be randomly distributed according to their average concentration ($x = 0.3$). Within the interfaces, however, the Al-Al correlation function has a long-range component which is due to the island formation during growth. On a reduced spatial grid we have solved the full four-dimensional electron-hole problem within the QW plane, using the time evolution of the inhomogeneous exciton equation [5]. In this way we were able to check if the factorization between in-plane COM and relative motion in Eq. (2) is justified or not. For the present parameters, the agreement is reasonably good in the $1s$ region (Fig. 2, right part). Around $E = 0$ (confinement gap), higher excited exciton states as well as the Sommerfeld-enhanced continuum show up which is clearly outside the $1s$ factorization Ansatz.

ALLOY AND INTERFACE DISORDER

Knowing about the specific correlations at the interfaces, we consider the following simple model which allows to disentangle alloy and interface disorder more clearly. We assume that a random uncorrelated alloy of constant concentration $\langle A(\mathbf{r})\rangle = x_0$ fills the barrier up to the interface $z = h(\mathbf{R})$ which gives

$$\eta(\mathbf{R}, z) = \Theta(h(\mathbf{R}) - z) \, A(\mathbf{R}, z) \; ; \quad A(\mathbf{r}) = 1 \text{ resp. } 0 \; . \tag{7}$$

Here, the interface has been characterized by thickness fluctuation h and correlation length ζ via

$$\langle h(\mathbf{R}) h(\mathbf{R}')\rangle = h^2 \exp(-|\mathbf{R} - \mathbf{R}'|^2/2\zeta^2) \; . \tag{8}$$

For small h, the in-plane Al-Al correlation can be cast into (V_0 - cation volume)

$$\begin{aligned} &\langle [\eta(\mathbf{R}, z) - x(z)] \, [\eta(\mathbf{R}', z') - x(z')]\rangle = \\ &x(z) \, (1 - x_0) \, V_0 \, \delta(\mathbf{r} - \mathbf{r}') \; + \; x_0^2 \, \delta(z) \, \delta(z') \, \langle h(\mathbf{R}) h(\mathbf{R}')\rangle \end{aligned} \tag{9}$$

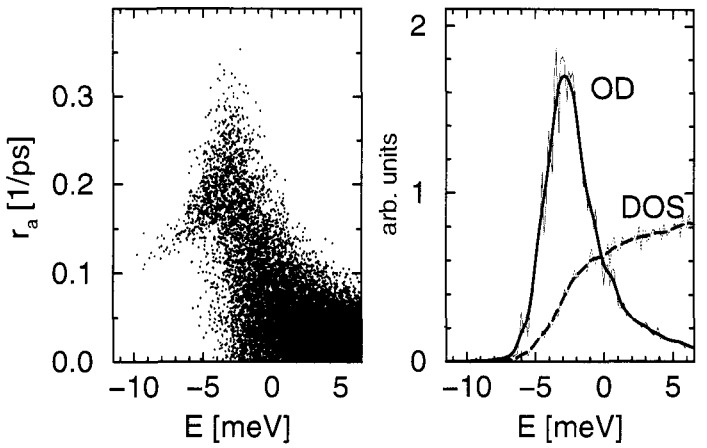

Fig. 3: Distribution of radiative rates (left) and resulting optical density (OD) compared with the excitonic density of states (DOS) (right). AlGaAs quantum well simulation with $L_z = 5\,\mathrm{nm}$ and $\sigma = 8\,\mathrm{meV}$.

and used to evaluate the potential variance $\sigma^2 = \langle V^2(\mathbf{R})\rangle$. The first term on the RHS of Eq. (9) is due to alloy disorder in an ideal structure, whereas the second one has to be identified with the interface roughness, and we may split the variance as $\sigma^2 = \sigma^2_{\mathrm{alloy}} + \sigma^2_{\mathrm{interfaces}}$. Adopting an exponential exciton $1s$ wave function with Bohr radius a_{B} exceeding the interface correlation length ζ, we get

$$\sigma^2_{\mathrm{alloy}} = \frac{V_0(1-x_0)}{2\pi a_{\mathrm{B}}^2}\left[K_{ee}\beta_e^2 + 8K_{eh} + K_{hh}\beta_h^2\right] ; \tag{10}$$

$$K_{ab} = \Delta_a\,\Delta_b \int dz\, u_a^2(z)\, u_b^2(z)\, x(z) .$$

Closely related expressions have been derived for alloy-broadening of excitons in bulk mixed crystals [6] and in ternary QWs [7].

For the interface part, application of $x_0\,\Delta_a\,u_a^2(0) = |dE_a/dL_z|$ leads to

$$\sigma^2_{\mathrm{interfaces}} = \frac{2h^2\zeta^2}{a_{\mathrm{B}}^2}\left((E_e'\beta_e)^2 + 8E_e'E_h' + (E_h'\beta_h)^2\right) . \tag{11}$$

In both cases, the energetic fluctuations of the COM potential are reduced by the ratio between statistically independent volume and exciton averaging volume [8], here $(a_{\mathrm{B}}^2 L_z)$. Therefore, a direct assignment of σ or exciton linewidth to the energy fluctuations on an atomic scale is not possible. The product $h \cdot \zeta$ entering Eq. (11) can be interpreted as island height times size. Upon growth interruption in the MBE process, h is expected to decrease, whereas ζ gets larger. Therefore, it is not clear a priori if growth interruption leads to a reduction of linewidth or not [9]. If eventually ζ exceeds the exciton radius a_{B}, the exciton line splits into a multiplett related to discrete monolayer energies. The present theory could be extended to that case, too.

EXCITON KINETICS AND LUMINESCENCE

The spontaneous radiation emitted from an exciton state α is proportional to its occupation N_α and its radiative recombination rate r_α. Apart from a constant prefactor, the luminescence intensity at frequency ω follows from summing over states as

$$I(\omega) = \sum_\alpha r_\alpha\, N_\alpha\, \pi\, \delta(\hbar\omega - \mathcal{E}_\alpha) . \tag{12}$$

The decay rate r_α (inverse radiative lifetime of state α) is given by [10]

$$r_\alpha = \frac{8ne^2\omega_x}{3\hbar c^3} P^2 \left| \int d\mathbf{r}\, \Psi_\alpha(\mathbf{r},\mathbf{r}) \right|^2 \tag{13}$$

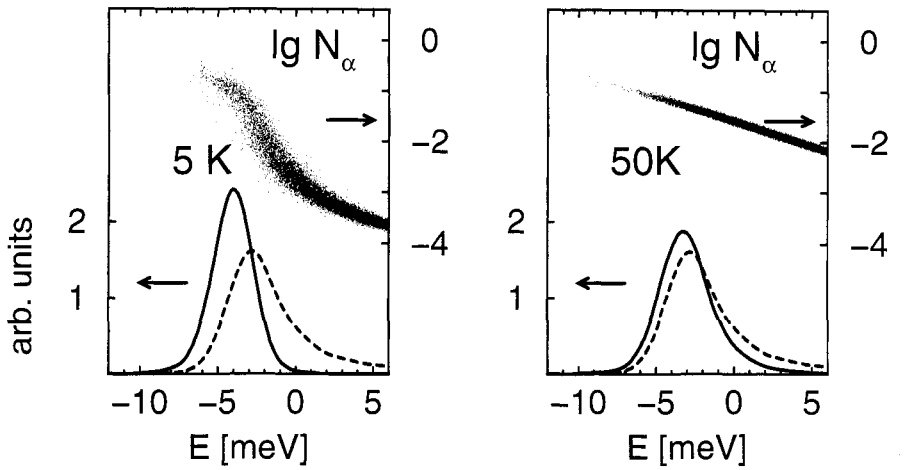

Fig. 4: Exciton kinetics in a QW with interface roughness (σ = 8 meV, a_B = 11 nm). Full curves – PL, dashed curves – OD, and occupation N_α on a logarithmic scale. Inelastic exciton scattering via acoustic phonons held at T = 5 K (left) and T = 50 K (right).

with Kane's interband momentum matrix element P and the index of refraction n. As in Eq. (5), the only state-dependent ingredient is the optical matrix element M_α^2. Throughout this section, parameters for a single GaAs QW with L_z = 5 nm embedded into $Al_{.3}Ga_{.7}As$ barriers are used. If M_α is given in nm we have $r_\alpha = M_\alpha^2 \cdot 1.7 \cdot 10^7\,\mathrm{s}^{-1}$. The distribution of radiative rates is shown in Fig. 3. Polariton effects in QWs dictate that all excitons with in-plane COM momentum between zero and $q_{\max} = \omega_x/c'$ are able to recombine radiatively [11]. We have checked that in our present simulation the typical wave function localization lengths obey $l_{\mathrm{loc}}\, q_{\max} < 1$, and therefore the simplified expression Eq. (13) holds perfectly.

The new quantity to be determined for the luminescence is the exciton occupation N_α. At low excitation, complete thermal equilibrium would result in a Boltzmann distribution $N_\alpha \sim \exp(-\mathcal{E}_\alpha/k_BT)$, but we expect strong deviations in particular at low temperatures. The competing mechanisms are thermally activated exciton transfer to the next available quantum state and the finite exciton lifetime. This can be described by a kinetic equation

$$\partial_t N_\alpha = G_\alpha + \sum_\beta \gamma_{\alpha\leftarrow\beta}\, N_\beta - (r_\alpha + \sum_\beta \gamma_{\beta\leftarrow\alpha})\, N_\alpha \tag{14}$$

which is linear in the occupation since we consider low excitation conditions (exciton-exciton interaction can be neglected). For excitation high in the band, the rapid initial cooling via emission of LO optical phonons can be visualized as a nearly state-independent generation rate $G_\alpha = I_0$. Below the LO threshold, the final inelastic scattering is due to acoustic bulk-like phonons with linear dispersion $\omega_q = u\,q$, following Takagahara [12]. Using standard deformation potential interaction and the factorization of the total exciton wave function Eq. (2), the transition rate can be written as

$$\gamma_{\alpha\leftarrow\beta} = W(\mathcal{E}_\alpha - \mathcal{E}_\beta) \int d\mathbf{R}\, \psi_\alpha(\mathbf{R})^2\, \psi_\beta(\mathbf{R})^2\,, \tag{15}$$

where the simplifying assumption of mainly in-growth momentum transfer to the phonon has been made (note that L_z is smaller than the characteristic in-plane length a_B). The spatial overlap between initial and final exciton state is crucial for the magnitude of the phonon scattering rate. Taking here realistic wave functions from the simulation improves over earlier attempts with ad hoc localized wave functions [12]. The scattering form factor

$$W(E) = \frac{n(E)\,E}{\hbar^2 u^3 \rho}[D_c K_e(q_z) - D_v K_h(q_z)]^2\,; \quad q_z = E/\hbar u \tag{16}$$

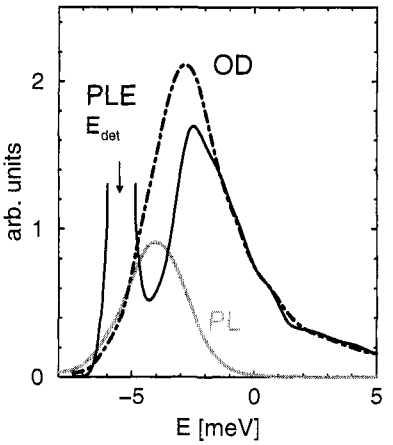

Fig. 5: Simulated photoluminescence excitation spectrum (PLE) in comparison with luminescence (PL) and optical density (OD). $T = 5$ K, other parameters as in Fig. 4.

contains the phonon distribution function $n(E) = (\exp(E/k_BT) - 1)^{-1}$ taken in equilibrium. Apart from bulk material parameters (deformation potential constants D_a, sound velocity u, mass density ρ) the Fourier transform of the confinement wave function u_a enters,

$$K_a(q_z) = \int dz\, e^{iq_z z} u_a^2(z)\,. \tag{17}$$

Simulation results for the steady state luminescence are displayed in Fig. 4 as full curves and compared with the optical density (dashed curves). The Stokes shift between PL and OD maximum is clearly seen, together with a reduction in linewidth. The individual occupation of states is visualized by plotting points N_α over $\mathcal{E}_\alpha$ on a logarithmic scale. At elevated temperatures this is close to the Boltzmann distribution since all states can frequently emit and absorb phonons to reach equilibrium. At lower temperatures, effective equilibration is restricted to the high-energy states which have a large wave function extension (band-like transport). But below the line center, localization gets more important, and the phonon transition between such tail states residing in different regions is hindered by an exponentially small overlap (hopping transport). Within the radiative lifetime, these states cannot equilibrate, and their occupation is dominated by the radiative rate being not much energy dependent. Although there is some spread in N_α one may think of a relaxation mobility edge, and the curvature of the occupation around the edge is responsible for the shrinkage of the PL linewidth. The present results justify on a microscopic level the two-class exciton kinetic model introduced recently [13] to interpret PL spectra in II-VI semiconductor QWs.

Near zero temperature the calculated PL lineshape compares rather well with a classical kinetic description due to Wilkinson et al. [14] who assumed that all excitons have time to "roll" into the nearest minimum of a disordered potential landscape, and could derive analytically the probability to find relative minima at a given energy. We have refined this idea [15] by including the basin of attraction which determines the number of excitons recombining at the bottom of a given minimum. Experimental data confirm a rather universal proportionality between Stokes shift and halfwidth [14] which is a persistent feature of both the classical as well as the quantum mechanical treatment of the disorder which is here presented for the first time. Surprisingly, the kinetic simulations showed a slight initial downshift of the Stokes shift S with increasing temperature before turning into the inverse temperature dependence as expected in equilibrium, $S^{\rm eq} = -\sigma^2/k_BT$. The non-monotonous behaviour of the Stokes shift is due to excitons which escape from shallow higher states by thermal activation and get trapped in deeper states before recombination. Recent luminescence experiments on ultrathin InAs quantum layers are in qualitative agreement [16].

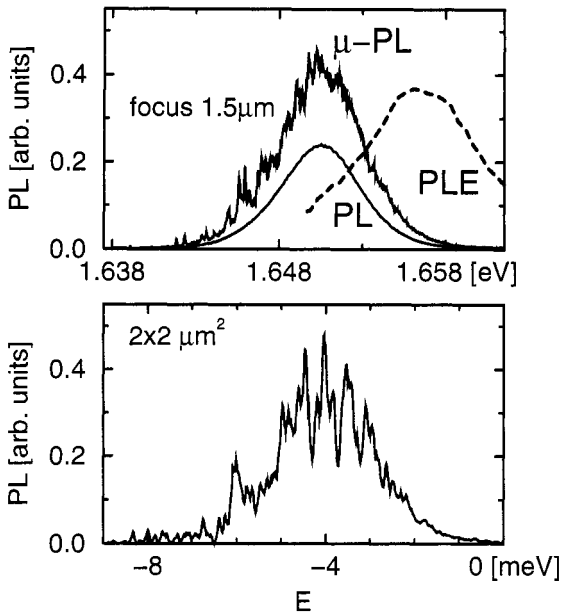

Fig. 6: Experimental micro-PL, PL, and PLE spectra of a 3.5 nm thick AlGaAs quantum well at $T = 5$ K (top) compared with a micro-PL simulation (bottom).

With a slight modification of the source term in the kinetic equation

$$G_\alpha = I_0 \, r_\alpha \, \delta_\Gamma(\mathcal{E}_\alpha - \hbar\omega_{\rm exc}) \tag{18}$$

we are able to simulate photoluminescence excitation (PLE) spectra as well. The delta function with subscript Γ is understood to describe the finite spectral range of the excitation, containing the spectral resolution as well as the homogeneous line width. The luminescence is now calculated and plotted as a function of the excitation energy $\hbar\omega_{\rm exc}$ with the detection energy held fixed (arrow in Fig. 5). At energies above the "relaxation mobility edge" OD and PLE agree fairly well, but below there is a significant drop in the PLE. Here, the excitation cannot be transfered easily from the excited states to the detection states within the exciton lifetime. The huge peak at $\hbar\omega_{\rm exc} = \hbar\omega_{\rm det}$ (not plotted in the Figure) is due to states which are resonantly excited and emitting, it is nothing else than resonant Rayleigh scattering via disorder in the present exciton system [17].

SPATIALLY RESOLVED LUMINESCENCE

In the numerical solution of the COM Schrödinger equation, the available simulation size is restricted by computer memory, and typically a grid of 100 x 100 discrete space points can be handled. Consequently, only a limited number of disorder eigenstates with large optical rate exists there, and the calculated optical spectra consist of seperate lines. Only after averaging the spectra over a number of different realizations smooth curves evolve as seen in common optical experiments. However, there has been recently an increasing interest in spatially resolved optical methods which allows to look at the exciton states individually. Scanning the sample surface with a glas fiber tip in near-field geometry is one of the possibilities. It has been demonstrated that the standard PL lineshape is nothing else than the envelope of many distinct lines related to localized exciton states [18, 19].

We concentrate here on the so-called micro-photoluminescence (micro-PL) which uses a microscop to focus the optical excitation and/or detection on the sample surface. Although its spatial resolution is typically of the order of 1 μm only, it gives a reproducible "spiky" spectrum where every peak can be related to an exciton COM eigenstate. Our numerical simulation without subsequent averaging

is therefore well adopted to this situation. In Fig. 6 (top) we reproduce a measurement of micro-PL in comparison with a large-focus PL [20]. The simulated micro-PL spectra (bottom) has been generated using parameters relevant to the experiment. A closer look on the spike distribution in the experiment as well as in the calculation shows a distinct dependence on energy: Whereas in the low-energy tail a few spikes with large weight dominate, the spikes become more frequent but less strong in the upper part of the spectra. We relate this to the quantum-mechanical nature of the underlying disorder eigenstates: There are only a few states in the tail which, however, are mostly local ground states exhibiting a relatively large optical matrix element. The increasing number of states towards the line center is counterbalanced by their small matrix elements (see Fig. 3). Due to this energy dependence of the spike structure it is not easy to extract something like an "average number of radiative states per unit area". However, a comparison with detailed calculations can give access to the distribution of localized exciton states. Even more information can be extracted if a statistical analysis of the energetic distances between spikes is carried out. Within further work, we will relate these findings to general theorems on level distance distributions in quantized systems. The exciton states in semiconductor nanostructures with disorder could provide a new example of this actual topic.

ACKNOWLEDGMENTS

Part of this work has been supported by the Deutsche Forschungsgemeinschaft in the frame of Sfb 296.

REFERENCES

1. G. Bastard, *Wave mechanics applied to semiconductor heterostructures*, Les Editions de Physique, Paris (1988).
2. F. Große and R. Zimmermann, *Superl. and Microstr.* **17**, 439 (1995).
3. R. Zimmermann and E. Runge, *J. Luminescence* **60&61**, 320 (1994); *SPIE Vol.* **2139**, 280 (1995); *Proc. 22nd ICPS Vancouver*, ed. D.J. Lookwood (World Scientific, 1995) p. 1424.
4. J. Köhler, A.M. Jayannavar and P. Reineker, *Z. Phys. B* **75**, 451 (1989).
5. S. Glutsch, D.S. Chemla and F. Bechstedt, *accepted by Phys. Rev. B.*
6. S.K. Lyo, *Phys. Rev. B* **48**, 2152 (1993).
7. S.D. Baranovskii, U. Doerr, P. Thomas, A. Naumov and W. Gebhardt, *Solid State Comm.* **89**, 5 (1994).
8. R. Zimmermann, *J. Crystal Growth* **101**, 346 (1990).
9. D. Bimberg, F. Heinrichsdorff, R.K. Bauer, D. Gerthsen, D. Stenkamp, D.E. Mars and J.N. Miller, *J. Vac. Sci. Technol. B* **10**, 1793 (1992).
10. U. Bockelmann, *Phys. Rev. B* **48**, 17637 (1993).
11. D.S. Citrin, *Phys. Rev. B* **47**, 3832 (1993).
12. T. Takagahara, *Phys. Rev. B* **31**, 6552 (1985).
13. U. Neukirch, D. Weckendrup, W. Faschinger, P. Juza and H. Sitter, *J. Crystal Growth* **138**, 849 (1994).
14. M. Wilkinson, Fang Yang, E.J. Austin and K.P. O'Donell, *J. Phys. C* **4**, 8863 (1992).
15. E. Runge, A. Schülzgen, F. Henneberger and R. Zimmermann, *phys. stat. sol. (b)* **188**, 547 (1995).
16. J.-L. Lazzari, R. Klann, *to be published.*
17. R. Zimmermann, *Il Nuovo Cimento* **17 D**, 1801 (1995).
18. H.F. Hess, E. Betzig, T.D. Harris, L.N. Pfeiffer and K.W. West, *Science* **264**, 1740 (1994).
19. K. Brunner, G. Abstreiter, G. Böhm, G. Tränkle and G. Weimann, *Appl. Phys. Lett.* **64**, 3320 (1994).
20. U. Jahn, S.H. Kwok, M. Ramsteiner, R. Hey, H.T. Grahn and E. Runge, *submitted to Phys. Rev. B.*